Kinetic Understanding of Neoclassical Scrape-off Layer Physics, Comparison with Fluid Modeling, and Experimental Validation

R.M. Churchill[1], J.M. Canik[2], C.S. Chang[1], R. Hager[1], A.W. Leonard[3], R. Maingi[1], R. Nazikian[1] and D.P. Stotler[1]

[1]Princeton Plasma Physics Laboratory, 100 Stellarator Road, Princeton, NJ 08540, USA
[2]Oak Ridge National Laboratory, PO Box 2008, Oak Ridge, TN 37831, USA
[3]General Atomics, PO Box 85608, San Diego, CA 92186-5608, USA

Corresponding Author: rchurchi@pppl.gov

Abstract:

Simulations using the fully kinetic neoclassical code XGCa were undertaken to explore the impact of kinetic effects on scrape-off layer (SOL) physics in DIII-D H-mode plasmas. XGCa is a total-f, gyrokinetic code which self-consistently calculates the axisymmetric electrostatic potential and plasma dynamics, and includes modules for Monte Carlo neutral transport.

Previously presented XGCa results showed several noteworthy features, including large variations of ion density and pressure along field lines in the SOL, experimentally relevant levels of SOL parallel ion flow (Mach number$\sim$0.5), skewed ion distributions near the sheath entrance leading to subsonic flow there, and elevated sheath potentials [R.M. Churchill, *Nucl. Mater. & Energy*, submitted].

In this paper, we explore in detail the question of pressure balance in the SOL, as it was observed in the simulation that there was a large deviation from a simple total pressure balance (the sum of ion and electron static pressure plus ion inertia). It will be shown that both the contributions from the ion viscosity (driven by ion temperature anisotropy) and neutral source terms can be substantial, and should be retained in the parallel momentum equation in the SOL, but still do falls short of accounting for the observed fluid pressure imbalance in the XGCa simulation results.

1 Introduction

Scrape-off layer (SOL) physics in tokamak devices are typically simulated using fluid codes, due to the generally high collisionality in this region. However, research has revealed a number of discrepancies between experiment and leading SOL fluid codes (e.g. SOLPS), including underestimating outer target temperatures[1], radial electric field in the SOL[2,

3, 1], parallel ion SOL flows at the low field side[4, 3, 5], and impurity radiation[6]. It was hypothesized by Chankin et al.[3] that these discrepancies stem from the use of a fluid code, ignoring kinetic effects particularly on parallel transport in the SOL.

To determine the importance of kinetic effects in the SOL, simulations were undertaken using the XGCa code[7], a total-f, gyrokinetic code which self-consistently calculates the axisymmetric electrostatic potential and plasma dynamics, and includes modules for Monte Carlo neutral transport. General features of the simulation results are investigated for kinetic effects, but also in the future comparisons will be made to the fluid SOL transport code SOLPS[8]. We note here that the present study is without turbulence. Turbulence may alter the results presented here.

Here we review previously presented findings from the XGCa simulation, focusing on differences with typical fluid results. We also focus on the question of parallel pressure balance in a low-density, low-power DIII-D H-mode plasma. A significant deviation from standard total pressure balance ($p_e + p_i + m_i n_i V_{i,\|}^2 = const$) occurs in the SOL of these XGCa simulations, and here we explore whether the addition of main ion viscosity and neutral source terms can account for this deviation.

The rest of the paper is organized as follows: Section 2 briefly describes the XGCa code, Section 3 details some of the simulation setup, Section 4 describes previously presented results, Section 5 discusses details of the pressure balance parallel to magnetic field lines, including main ion viscosity and neutral source terms, and Section 6 wraps up with conclusions and plans for future work.

2 XGCa

XGCa is a total-*f*, gyrokinetic neoclassical particle-in-cell (PIC) code[7, 9, 10]. The ions are pushed according to a gyrokinetic formalism, and the electrons are drift-kinetic. XGCa is very similar to the more full featured, gyrokinetic turbulence version XGC1[9, 11, 10], the main difference being that XGCa solves only for the axisymmetric electric potential (i.e. no turbulence, hence the "neoclassical" descriptor). An important feature of XGCa is that the poloidally varying electric potential is calculated by solving a gyrokinetic Poisson equation, so that the resulting electric field is self-consistent with the gyrating kinetic particles. XGCa also uses a realistic magnetic geometry, created directly from experiment magnetic reconstructions (normally from EFIT EQDSK files), including X-points and material walls. Particle drifts (magnetic and $E \times B$) are included on the particle motion. Kinetic effects of neutrals from charge-exchange and ionization are included, along with consistent neutral rates set by global recycling. The Debye sheath region isn't resolved, but rather a logical sheath boundary condition[12, 13] is used to impose ambipolar flux to the material walls. There are two main differences between XGCa and the previous neoclassical version XGC0. XGC0 calculates only flux-averaged potential and includes the gyro-averaging effect in a simplified manner.

3 XGCa Simulation Setup

The results presented in this paper are from an XGCa simulation of a low-power H-mode discharge of the DIII-D tokamak[14], shot 153820 at time 3000 ms. The simulation parameters, including experimental inputs of ion and electron density and temperature, can be found in Ref. [12]. This discharge was chosen for its lower density, so that the SOL collisionality would be low, where kinetic effects would be expected to be more significant (so called "sheath-limited" regime).

4 Previous Results

Here we briefly summarize a few key results previously presented and published [12].

First, the ion density and temperature exhibit significant poloidal variation in the SOL. Plots of the density (since no impurities are used in the simulation, $n_e = n_i$), and ion temperature in normalized poloidal flux (ψ_n) versus poloidal length along a flux surface (L_θ) space are shown in Figure 1. The difference in the poloidal variation of n_i and T_i is suggestive of the fact that fat orbits of higher energy ions is centered closer to the LFS midplane, whereas a larger fraction of ions exit closer to the X-point.

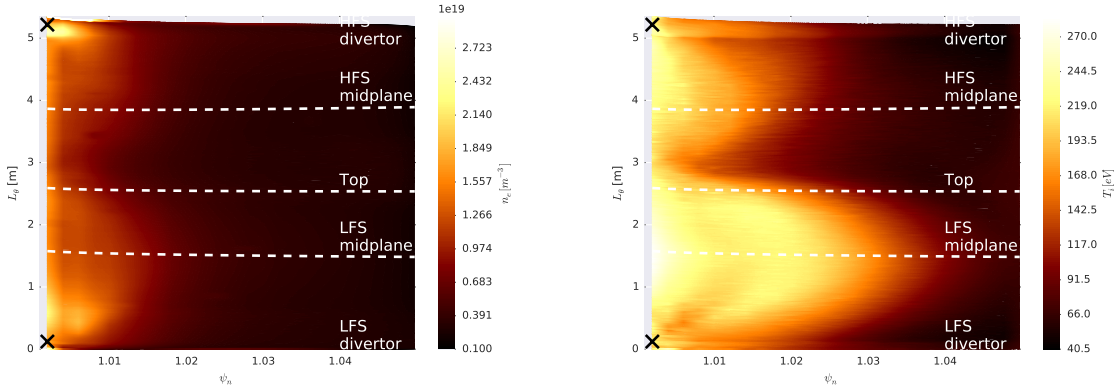

(a) *(b)*

FIG. 1. (a) Electron density and (b) ion temperature poloidal variation in the SOL. The x-axis is the normalized magnetic flux, ψ_N, and the y-axis is the poloidal distance along a flux surface, L_θ, with 0 at the LFS divertor, increasing poloidally towards the HFS divertor. Recognizable features such as midplane and divertor are marked by the white dashed lines, and the X's on the y-axis indicate where the X-point is.

Second, the XGCa simulated parallel ion flow in the SOL is at experimentally relevant magnitude[4, 5, 3, 15] ($M_i \sim 0.5$). The parallel ion flow also exhibits significant poloidal variation, with stagnation points near the top of the machine, and near the divertor plates[16]. Figure 2 shows the parallel ion flow Mach number in the SOL ($M_{i,\|} = V_{i,\|}/c_s$, where $c_s = \sqrt{(T_e + T_i)/m_i}$ is the sound speed). The main driver which would account for the realistic $M_{i,\|}$ levels in XGCa, and which contrasts to fluid codes, would appear

to be the radial electric field, E_r, which is solved for using the full gyrokinetic Poisson equation. This would be consistent with work which showed that including the experimentally measured E_r in a simplified equation for the Pfirsch-Schlütter flow recovers the experimentally measured SOL parallel ion Mach number at the LFS midplane[2].

Lastly, the Debye sheath potential calculated with the logical sheath boundary condition is higher than would be expected from a simple analytic formula[17], shown in Figure 3a. The values for $e\Phi_{sh}/T_e$ range from 3-4 over most of the SOL, while the expected value based on Maxwellian fluxes for this discharge is almost a constant 2.5 over the entire SOL.

Two simple observations can qualitatively account for the elevated sheath potentials. First, while the electron distribution is close to Maxwellian at the sheath edge, there is a small tail of high energy electrons; these high-energy electrons ultimately determine the sheath potential, with the rest of the electrons being reflected out of the sheath. Second, the ion distribution function f_i at the edge, shown in Figure 3b, has a negative skewness, es-

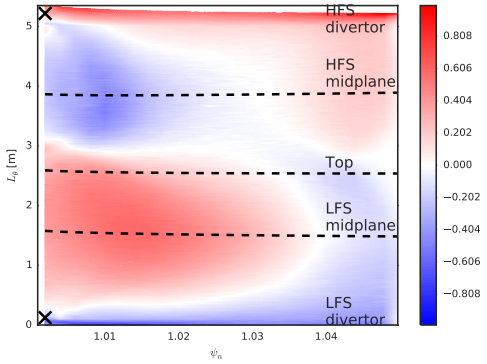

FIG. 2. Contour plot of neoclassical parallel Mach number ($M_{i,\|} = V_{i,\|}/c_s$) in the SOL. Axes are the same as Figure 1. Color indicates $M_{i,\|}$ strength: red being towards the HFS divertor, blue towards the LFS divertor, and white stagnation points.

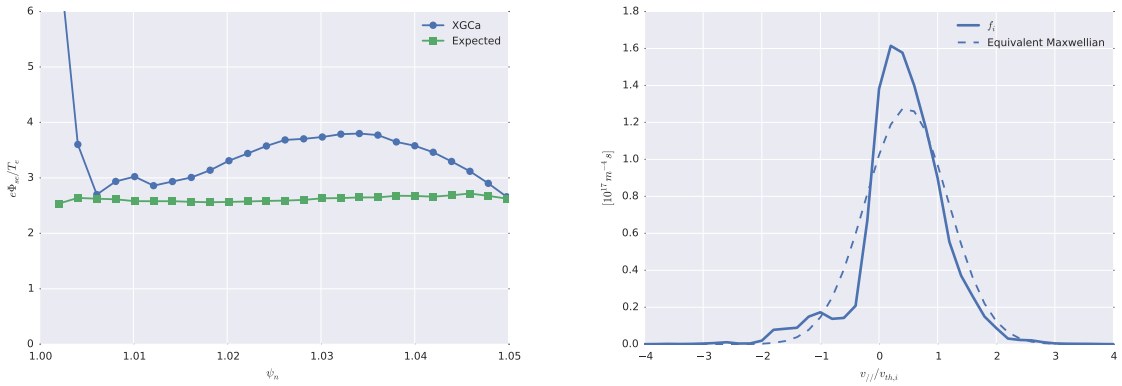

(a) *(b)*

FIG. 3. (a) Normalized sheath potential versus ψ_N. The XGCa sheath potential is shown in blue circles, the expected sheath potential is shown in green squares. (b) Ion distribution function at the sheath edge versus normalized parallel particle velocity, near $\psi_n = 1.03$. f_i from XGCa is shown in solid, and an equivalent Maxwellian (same n_i, T_i and V_i) is shown in dashed lines

pecially when only considering the forward going particles ($v_\parallel > 0$). The *one-way* flux Γ_i^+ of f_i into the sheath is smaller than the one-way flux from a Maxwellian (pictured in Figure 3b with equivalent n_i, V_i, and T_i). This skewed distribution allows for a subsonic $V_{i,\parallel}$ at the sheath edge while still satisfying ambipolar flux into the sheath.

5 Pressure Balance

Pressure balance in the SOL ($p_e + p_i + m_i n_i V_i^2 = const$) is often used to derive expected target plasma profiles, for example using two-point modeling[17]. For small midplane ion flows, and target flows satisfying the Bohm criterion ($V_{i,\parallel} = c_s$), the midplane static pressure ($p_e + p_i$) should be 2x the divertor static pressure[17]. SOL measurements of upstream n_e, T_e, and T_i, with downstream n_e and T_e done in DIII-D attached ELMing H-mode plasmas showed[18] seem to agree with this. However, assumptions of low midplane flows and $T_i \approx T_e$ in the divertor had to be made, since main ion measurements are notoriously difficult to measure in the SOL generally.

As a simple test, the total pressure ($p_e + p_i + m_i n_i V_{i\parallel}^2$) in the SOL from this XGCa simulation is plotted in Figure 4a, normalized to the LFS target total pressure. A large imbalance is seen, ranging from near balanced in the farthest out flux surfaces (yellow) to factors of 2.5 for flux surfaces in the near-SOL (blue). Here we consider adding the momentum drag from neutrals and the main ion viscosity into the parallel momentum equation. As will be seen, these simple fluid terms cannot account for the pressure imbalance from the kinetic simulation, requiring future work on a more complete fluid momentum balance equation.

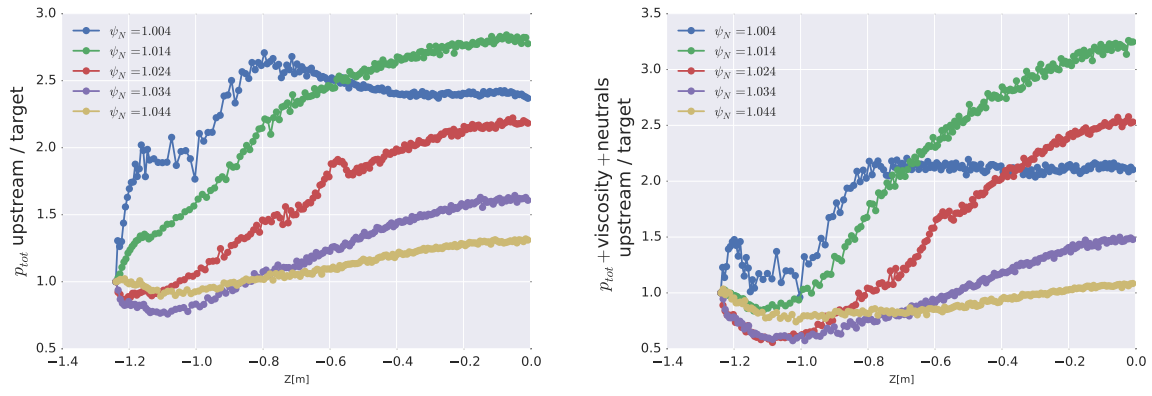

(a) *(b)*

FIG. 4. Figure 4a shows the ratio (upstream over target) of total pressure ($p_e+p_i+m_i n_i V_{i\parallel}^2$) between the LFS divertor target and upstream midplane, plotted versus height (Z). Figure 4b shows pressure balance using Equation 2, showing that adding main ion viscosity and neutral sources cannot account for the total pressure imbalance.

5.1 Parallel Momentum Equation

A total parallel momentum equation[19, 20] can be formed using the procedure and assumptions outlined in Ref. [19], arriving at:

$$\mathbf{b}\cdot[m_i n_i \mathbf{V}_i\cdot\nabla\mathbf{V}_i + \nabla(p_e+p_i) + \nabla\cdot\pi_i] + m_i V_{i,\parallel} n_n\left(\nu_{ion}+\nu_{cx}\right) = 0 \quad (1)$$

where $\nu_{ion} = n_e\langle\sigma_{ion}v\rangle$ and $\nu_{cx} = n_i\langle\sigma_{cx}v\rangle$ are the ionization and charge exchange rates. We further simplify the ion inertia term as $\mathbf{b}\cdot\mathbf{V}_i\cdot\nabla\mathbf{V}_i = \mathbf{b}\cdot\nabla(V_i^2/2) - \mathbf{V}_i\times\nabla\times\mathbf{V}_i \approx \mathbf{b}\cdot\nabla(V_i^2/2)$, noting that $\mathbf{V}_i\times\nabla\times\mathbf{V}_i$ can contain important terms. We also simplify the viscosity using only the parallel viscosity (neglecting perpendicular gyroviscosity) in the Chew-Golberger-Low form[20, 21], $\mathbf{b}\cdot\nabla\cdot\pi_{i\parallel} = \frac{2}{3}\mathbf{b}\cdot\nabla(p_{i\parallel}-p_{i\perp}) - (p_{i\parallel}-p_{i\perp})\mathbf{b}\cdot\nabla\ln B$. Substituting these simplifications, and integrating over the parallel direction from $\ell_\parallel = 0$ at the divertor target to x, an upstream value, we arrive at the final pressure balance in Equation 2.:

$$\frac{\left(p_{tot}+\frac{2}{3}(p_{i\parallel}-p_{i\perp})\right)|_{\ell_\parallel=x} + \int_0^x d\ell_\parallel\,\left[m_i V_{i\parallel} n_n(\nu_{ion}+\nu_{cx}) - (p_{i\parallel}-p_{i\perp})\mathbf{b}\cdot\nabla\ln B\right]}{\left(p_{tot}+\frac{2}{3}(p_{i\parallel}-p_{i\perp})\right)|_{\ell_\parallel=0}} = 1 \quad (2)$$

where we have written the total pressure as $p_{tot} = p_e + p_i + \frac{1}{2}m_i n_i V_i^2$.

5.2 Ion temperature anisotropy

Ion pressure anisotropy is the drive in the parallel viscosity term, which is not normally considered in fluid codes since strong collisionality would generally reduce anisotropies in confined plasmas. The kinetic XGCa simulation results show that there is a strong main ion temperature anisotropy in the SOL, beginning just inside the separatrix in the pedestal region, and increasing in the SOL. The plot of SOL $T_{i\parallel}/T_{i\perp}$ in Figure 5 shows the ion temperature (or more precisely the average kinetic energy) anisotropy ratio reaches levels of 0.25, but also has regions where $T_{i\parallel} > T_{i\perp}$, with the ratio as high as 1.35 at the top of the machine. The LFS region ion temperature anisotropy can be explained by a significant trapped ion fraction, which leads to a predominantly higher perpendicular energy. The region of $T_{i\parallel} > T_{i\perp}$ near the top is also due to kinetic effect with the higher parallel-energy ions flowing more freely to the top avoiding trapping at LFS. The low end anisotropy ratio is near the simple theoretical limit of ion viscosity[17] ($\pi_i > -p_i$), which translates to $p_{i\parallel}/p_{i\perp} > 2/5$.

5.3 Pressure balance updated

Using the contributions from the main ion viscosity and neutral source, we update the plot of Figure 4a, to plot the more complete pressure balance equation, Equation 2 in Figure 4b. As seen, there is a significant deviation from 1 for flux surfaces in the near- to mid-SOL. For the flux surfaces further in the far-SOL, where the collisionality is higher, the agreement is fairly good, deviating on the level of 10% between the target and midplane.

The pressure imbalance is dominated by the variation in the ion temperature, and so is likely due to not including kinetic effects from high energy ion contributions not included in this fluid picture. It is possible that including the in-surface flows in the inertia term ($\mathbf{V} \times \nabla \times \mathbf{V}$) can also be important, and needs to be explored.

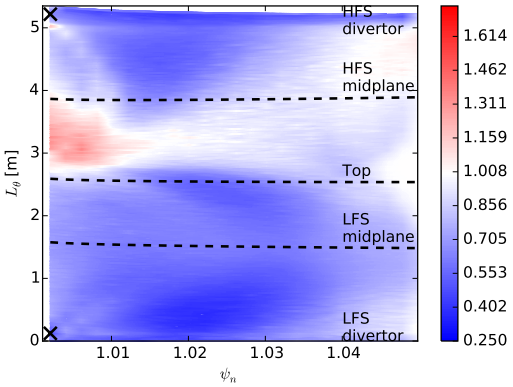

FIG. 5. Ion temperature anisotropy ratio, $T_{i\parallel}/T_{i\perp}$.

6 Conclusions and Future Work

Highlights from an XGCa simulation of a low-density DIII-D H-mode plasma, focused on understanding kinetic effects in the scrape-off layer were presented. The XGC codes are useful for probing and predicting kinetic effects in the edge region, including the scrape-off layer, as they include many of the interconnected physics necessary for realistic modelling. The ion density and temperature are larger at the LFS, indicating effects from fat ion orbits from the confined pedestal region. The parallel ion Mach number at the LFS midplane reaches experimental levels ($M_i \sim 0.5$), and shows a poloidal variation consistent with the parallel ion flows being dominated by Pfirsch-Schlütter flows (recall XGCa includes drifts), with stagnation points near the X-point at both the LFS and HFS and flows directed towards the divertor below the X-point. The normalized sheath potential at the divertor plates is higher than standard textbook assumptions, along with subsonic ions at the sheath edge, which both implicate kinetic effects in the establishment of the sheath potential in this discharge.

Pressure balance in the SOL of these simulations was explored, showing a strong deviation when using total pressure only. Significant ion temperature anisotropies are present in the pedestal and SOL of this simulation, indicating main ion viscosity could play a significant role in the pressure balance. Main ion viscosity and neutral source terms were included and, while significant in the SOL, they could not account for the entire fluid pressure imbalance seen in XGCa , especially for flux surfaces in the near- and mid-SOL.

The present physics results are without turbulence or impurity particles, leaving them for future work. Turbulence and impurity could modify the results presented here.

7 Acknowledgements

This work supported by the U.S. Department of Energy under DE-AC02-09CH11466, DE-AC05-00OR22725, and DE-FC02-04ER54698. Awards of computer time was provided by the Innovative and Novel Computational Impact on Theory and Experiment (INCITE) program. This research used resources of the Argonne Leadership Computing Facility, which is a DOE Office of Science User Facility supported under contract DE-AC02-06CH11357. This research also used resources of the National Energy Research

Scientific Computing Center, a DOE Office of Science User Facility supported by the Office of Science of the U.S. Department of Energy under Contract No. DE-AC02-05CH11231. DIII-D data shown in this paper can be obtained in digital format by following the links at https://fusion.gat.com/global/D3D_DMP

References

[1] CHANKIN, A. et al., J. Nucl. Mater. **390-391** (2009) 319.

[2] CHANKIN, A. et al., Nucl. Fusion **47** (2007) 479.

[3] CHANKIN, A. V. et al., Plasma Phys. Control. Fusion **51** (2009) 065022.

[4] ASAKURA, N., J. Nucl. Mater. **363-365** (2007) 41.

[5] GROTH, M. et al., Nucl. Fusion **49** (2009) 115002.

[6] CANIK, J. M. et al., J. Nucl. Mater. **463** (2015) 569.

[7] HAGER, R. et al., Phys. Plasmas **23** (2016) 042503.

[8] ROZHANSKY, V. et al., Nucl. Fusion **49** (2009) 025007.

[9] KU, S. et al., Nucl. Fusion **49** (2009) 115021.

[10] KU, S. et al., J. Comput. Phys. **315** (2016) 467.

[11] CHANG, C. S. et al., J. Phys. Conf. Ser. **180** (2009) 012057.

[12] CHURCHILL, R. et al., Nucl. Mater. Energy **submitted** (2016).

[13] PARKER, S. et al., J. Comput. Phys. **104** (1993) 41.

[14] LUXON, J. L. et al., Fusion Sci. Technol. **48** (2005) 807.

[15] BOEDO, J., J. Nucl. Mater. **390-391** (2009) 29.

[16] BOEDO, J. et al., J. Nucl. Mater. **266-269** (1999) 783.

[17] STANGEBY, P., *The Plasma Boundary of Magnetic Fusion Devices*, Institute of Physics Publishing, Bristol, 2000.

[18] PETRIE, T. et al., J. Nucl. Mater. **196-198** (1992) 848.

[19] CHURCHILL, R. M., *Impurity Asymmetries in the Pedestal Region of the Alcator C-Mod Tokamak*, Ph.d. thesis, Massachusetts Institute of Technology, 2014.

[20] HELANDER, P. et al., *Collisional transport in magnetized plasmas*, Cambridge University Press, 2005.

[21] SHAING, K. C. et al., Phys. Fluids B Plasma Phys. **5** (1993) 3596.